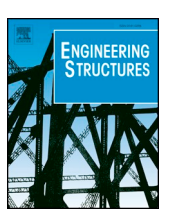
FISEVIER

Contents lists available at ScienceDirect

# **Engineering Structures**

journal homepage: www.elsevier.com/locate/engstruct



# Probabilistic performance assessment of power distribution infrastructure under wind events



Yee Er Teoh<sup>a</sup>, Alice Alipour<sup>b,\*</sup>, Alessandro Cancelli<sup>b</sup>

- <sup>a</sup> T.Y. Lin International, Selangor, Malaysia
- b Iowa State University, United States

#### ARTICLE INFO

Keywords:
Distribution poles
Wind load
Ice load
Life-cycle analysis
Mitigation

#### ABSTRACT

The electric power delivery infrastructure directly contributes to essential societal functions, the economy, and the general quality of life. Recent extreme wind events, such as Hurricanes Irma and Maria, and more recently Hurricane Michael resulted in power outages that affected millions of customers and led to major social and economic disruptions throughout communities. The longer the outage duration, the greater the incurred losses. Power distribution systems have proven to be highly vulnerable to such events and responsible for 90% of the outages. Distribution structures are built according to safety standards to ensure the safety of assets in operational and extreme conditions, but the dynamic nature of the wind loading is often overlooked or only considered empirically. Therefore, in this paper, such effects are included in a comprehensive risk-informed framework to assess the performance of electric power distribution components. This methodology explicitly accounts for the inevitable uncertainty in predictions of the component response. The focus is on characterizing wind events and the component-level risk analysis of physical components of the electric power system. For this purpose, a power pole-conductor system is modeled in which wind events are simulated as one-dimensional multivariable stochastic processes along the height of the poles and the conductors. Three-second peak gust wind speeds are used as a modeling reference. A probabilistic framework is developed to estimate the capacity of the distribution poles under different aging mechanisms. The response of the power distribution poles due to the simulated wind speeds is then computed using a finite element analysis. Fragility functions are generated to estimate the probability of exceedance for different damage states. A set of hazard mitigation strategies, the associated costs, and estimated benefits are implemented, and the improved fragility functions for elements are generated. A probabilistic life-cycle cost analysis is used to assess the long-term benefits of investing in different components of the power distribution system.

## 1. Introduction

In recent years, extreme weather events have led to widespread outages in the United States, resulting in significant socioeconomic costs [1,2]. The average total cost of these extreme weather events rose from \$20B per year in the 1980s to \$85B in the 2010s [3]. Extreme weather events contributed to 58% of U.S. grid outages, which resulted in annual economic losses of \$18B to \$33B from 2003 to 2012 [4]. In this period, 90% of the aforementioned outages in the U.S. were due to failures in distribution systems [5]. A power distribution system is the portion of an electric power system that delivers electric energy from transformation points on the high- and medium-voltage transmission system to customers and, more recently, from distributed energy resources (DER) such as wind turbines and rooftop solar panels back up to

the high-voltage transmission system (Fig. 1).

One major destructive event, Hurricane Katrina in 2005, carried a peak sustained wind speed of 77.79 m/s for 6 h and resulted in power outages that lasted up to several weeks, affecting 2.7 million customers in the southern United States [6–8]. Katrina destroyed 72,500 utility poles and damaged 8280 transformers and 1520 transmission structures, with 300 substations going out of service [8]. In September 2017, Category 5 Hurricanes Irma and Maria hit the United States with maximum sustainable wind speeds of 82.70 and 78.23 m/sec, respectively, destroying much of the electric power infrastructure and creating economic havoc, especially in Puerto Rico. Irma caused power outages for more than 8.7 million customers in the southern United States, whereas Maria left 95% of Puerto Rico without power. These recent events showed major vulnerabilities in the distribution system.

E-mail address: Alipur@iastate.edu (A. Alipour).

<sup>\*</sup> Corresponding author.

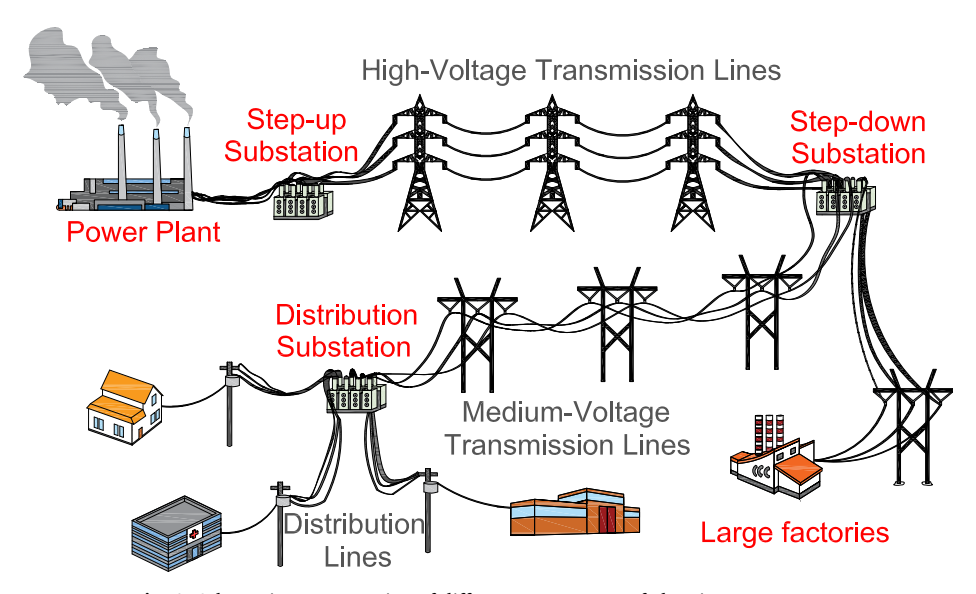


Fig. 1. Schematic representation of different components of electric power system.

Many studies have looked into electric power system damage due to hurricane winds. These can be divided into two main categories: component-level and network-level studies. The latter can be further subdivided into two methodologies: i) statistical models and prediction of network outages, and ii) analyses of network topological features. The first approach uses historical data to predict regional power outrages [9]; however, it does not provide any information about component-level failures. Methodologies based on topological features use network topology to measure network reliability [10-14]; nonetheless, they fail to account for hazard characteristics or exposure conditions that affect the network components and their level of risk exposure. More interesting for this study are component-level approaches, since they account for hazard data and provide engineering information on component-based failure risk. Typical studies have focused on a utility pole capacity analysis under wind, considering the effects of aging [15–17]. Although these approaches are common for catastrophic events such as hurricanes, limited study has been devoted to more common types of wind events that can also generate power outages. Among other risks for distribution systems, winter storms—such as blizzards or ice storms-produce snow, sleet, or freezing rain under low-temperature conditions that can lead to ice formation around overhead lines. Ice formation increases the weight of the lines and can cause the conductors or neutral wires to break, generating an unbalanced tension force in the pole along the longitudinal direction parallel to the distribution lines. The breakage of conductors disrupts the distribution system, and it could also cause outages up to several days or months depending on the repair and replacement time. Another effect of the ice layer is that it increases the surface area of the cables, which then generates additional wind-induced load on the pole and exposes the distribution system to increased failure risk. It is expected that the financial costs and societal impacts associated with weatherrelated power outages will keep increasing significantly, since historically rare weather events are now becoming more common and intense [2,18-20]. In addition, U.S. power grids are aged and outdated, making them more vulnerable to such events [21].

This study proposes an analysis framework for a distribution system under winter storm conditions. The system consists of poles composed of wood. This material decision is based on the wide usage of wood poles in distribution systems [22], mainly due to their ease of installation, low cost, and natural insulation properties [17]. Among these wooden poles, approximately 75% are made of Southern Pine [16,23]. Other types of material, such as steel, concrete, and fiber-reinforced polymer, have also been used in the field [24–26]. To ensure

the proper functionality of the distribution system, its physical components must be reliable and able to withstand wind events without large-scale or long-duration power outages in the serviced area. A well-maintained wooden power distribution pole has a life expectancy of about 70 years [27]. Most distribution poles are three-phase, four-wire systems, consisting of a triphasic transformer, three overhead conductors, and a neutral wire. The transformer is negligible when analyzing the system for wind effects, while the conductors are a source of prominent wind forces on the poles. The wind acting on the conductors generates forces directed along their span, which are balanced by the distribution poles. In turn, the poles are subjected to large tension forces along the direction of the wind. This force results in a significant bending moment at the base of the poles that could eventually reach the ultimate bending moment capacity, leading to pole failure.

The design of distribution lines is dependent on the maximum allowable wind span, which is calculated based on the loads on distribution poles. The loading on a distribution pole includes (i) the weight of the attached equipment, conductors, and neutral wires and the vertical load component of the guy tension force; (ii) tension forces from the conductors and neutral wire during the installation of new lines; and (iii) wind loadings on the pole, conductors, and neutral wire based on the wind span. The transverse horizontal load component, which is the wind loading perpendicular to the lines, typically governs the design of the distribution lines. Based on these loadings and the ultimate bending moment capacity of the selected wooden pole class and length, the maximum allowable wind span can be determined. This is the maximum separation distance for two distribution poles that also satisfies the structural performance safety criteria. However, when the distribution lines are designed according to the maximum allowable wind span, any possibility of future upgrade is lost. For example, no additional communication lines can be added to the poles, and larger conductors with higher current-carrying capacity cannot be upgraded. Each upgrade will increase the bending moment due to wind loadings, making the distribution line more vulnerable to wind-induced failure for the same wind span. It should be noted that, while the design procedure accounts for the span lengths, it considers a constant value for the wind speed. However, wind is a turbulent phenomenon that oscillates around a certain mean value, with peaks that can deviate significantly from the mean. Due to this characteristic and to the dynamic interaction between wind loading and structures, it is necessary to apply an analysis procedure that can include these effects.

This paper provides a probability-based approach to assessing the risk to distribution line components and provides a life-cycle cost

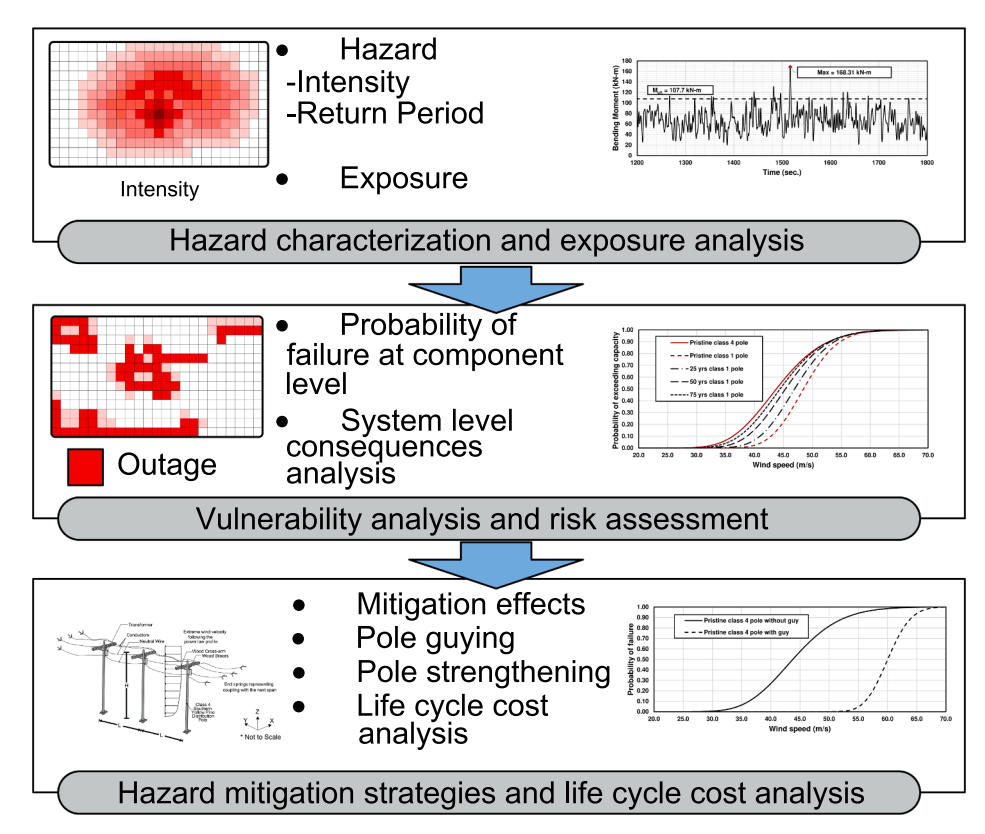


Fig. 2. The framework considered in this study.

analysis approach to the selection of appropriate mitigation strategies. The basis of the approach is hazard characterization, defined as the identification of hazard features such as its likelihood of occurrence and intensity. A vulnerability analysis for each identified hazard evaluates the vulnerability of different components of the power distribution with a probability-based approach. Such vulnerabilities are defined through a series of fragility functions for the different structures' components under varying aging scenarios. Using all this information, a risk assessment analysis estimates the probability of failure of the system components and its possible consequences. The proposed framework is also employed to evaluate the performance of asset-hardening strategies and their impact on vulnerability reduction in the system components. Lastly, a life-cycle cost analysis is employed to estimate the costs associated with failures and mitigation strategies throughout the life cycle of the system, yielding a complete framework that can be used as a tool for decision-making. Fig. 2 shows the components of the study. Section 2 of this paper presents the characterization of the wind and ice hazard, and Section 3 illustrates the model used to simulate wind time histories and the relative wind-induced load on the system. Section 4 defines the finite element model used to calculate the bending moment demand, the nominal resisting bending moment calculation procedure with aging effects, and the fragility functions for the pristine and decayed poles. Section 5 discusses different mitigation strategies, Section 6 introduces the life-cycle cost analysis approach to estimate the costs and benefits of using the mitigation strategies, and Section 7 concludes the paper and provides suggestions for future research.

# 2. Hazard characterization

As highlighted in the introduction, winter storms present a significant risk of failure to distribution poles due to a high wind load combined with the effects of ice formation. This section will illustrate in detail how both hazards were introduced into the proposed framework.

## 2.1. Ice formation

Section 25 of the National Electrical Safety Code (NESC) [28] specifies in detail how to address the possibility of ice formation during winter storms, especially with strong wind speeds. The NESC introduces different loading requirements depending on the pole height and location. For structures less than 18 m (60 ft) tall, the code (rule 250B) identifies four different loading districts, assuming varying ice thicknesses on the cables and the simultaneous presence of wind and ice. The designed loading categories are heavy, medium, light, and warm islands (refer to Table 250-1 of the NESC [28]).

#### 2.2. Wind speed

To fully characterize the wind hazard in a probabilistic framework, it is necessary to describe the wind speed occurrence using a probability density function (PDF) that accurately fits available data for the structure's site. In this study, such data are based on the ultimate wind loading due to gust wind speed as determined by Vickery et al. [29]. The Chicago area was selected as a case study, and Table 1 shows the area's peak wind speeds for different return periods [29]. To assess the

Table 1
Return period and peak gust wind speed obtained from Vickery et al. [29].

Return Period (years)	10	25	50	100	300	700	1700
Wind Speed in m/s (mph)	34.0 (76)	37.5 (84)	40.2 (90)	42.9 (96)	47.4 (106)	51.0 (114)	54.5 (122)

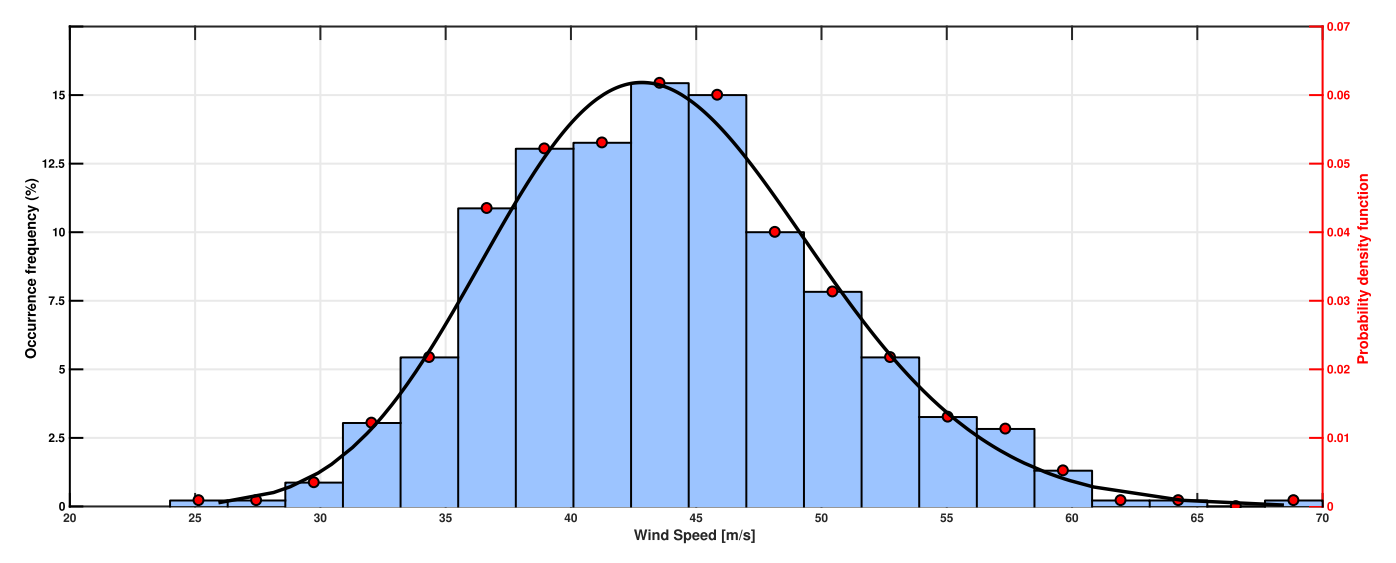


Fig. 3. Design gust wind speed Gamma distribution vs occurrence frequencies obtained with traditional sampling techniques for (a) 500 samples and (b) 5000 samples.

best fitting PDF for these data, the gamma, Weibull, normal, Gumbel, Rayleigh, and generalized extreme value (GEV) distributions were analyzed and the Kolmogorov–Smirnov (K-S) test was used to find the best fit for the data. Results showed that the gamma distribution produced the best fit for representing the wind speed in the region. Its probability density function (PDF) can be described using the following equation:

$$f(U_3|a,b) = \frac{1}{b^a \Gamma(a)} U_3^{a-1} e^{\frac{-U_3}{b}}$$
(1)

where  $U_3$  is the 3-second gust wind speed (m/s),  $\alpha$  is the shape parameter, b is the scale parameter, and  $\Gamma(a)$  is the gamma function.

To fully represent the wind speed hazard characterized by Eq. (1), it is necessary to draw a significant number of samples from the PDF so the full range of wind speeds can be explored. However, normal sampling techniques are not practicable due to the extremely elevated number of samples needed for a suitable representation. In fact, with a simple random number generator (RNG), a minimum of 5000 samples are needed to achieve an accurate representation of the PDF (Fig. 3). For this reason, this study uses Latin hypercube sampling (LHS) [30] to generate the wind sample, as LHS allows a drastic reduction in the samples needed to correctly represent the wind hazard. As shown in

Fig. 4, the histogram obtained from 500 samples using LHS compares well with a histogram of 5000 samples from regular sampling (Fig. 3). Therefore, 500 wind speed samples using the LHS technique was deemed to be an accurate representation of the wind hazard.

## 3. Wind load model

The 500 wind speed samples, defined above, are used as average values to create an artificially simulated time history of the wind event. This approach allows for a time-domain analysis of the system to account for the actual dynamic effect caused by the fluctuation of the wind speed on the pole and the conductors. The time history of the wind events for each wind realization is generated based on the stochastic field approach provided by Shinozuka and Deodatis [31]. For a given point, the wind fluctuation along the wind direction can be assimilated to a one-dimensional, one-variable (1D-1V) stochastic process  $f_0(t)$  with zero mean, two-sided power spectral density function  $S^0(\omega)$ , and it can be simulated with an infinite series of cosine functions as follows:

$$f(t) = \sqrt{2} \sum_{n=0}^{N-1} A_n \cos(\omega_n t + \phi_n), A_n = (2S^0 \omega_n \Delta \omega)^{1/2}, \omega_n = n\Delta \omega$$
 (2)

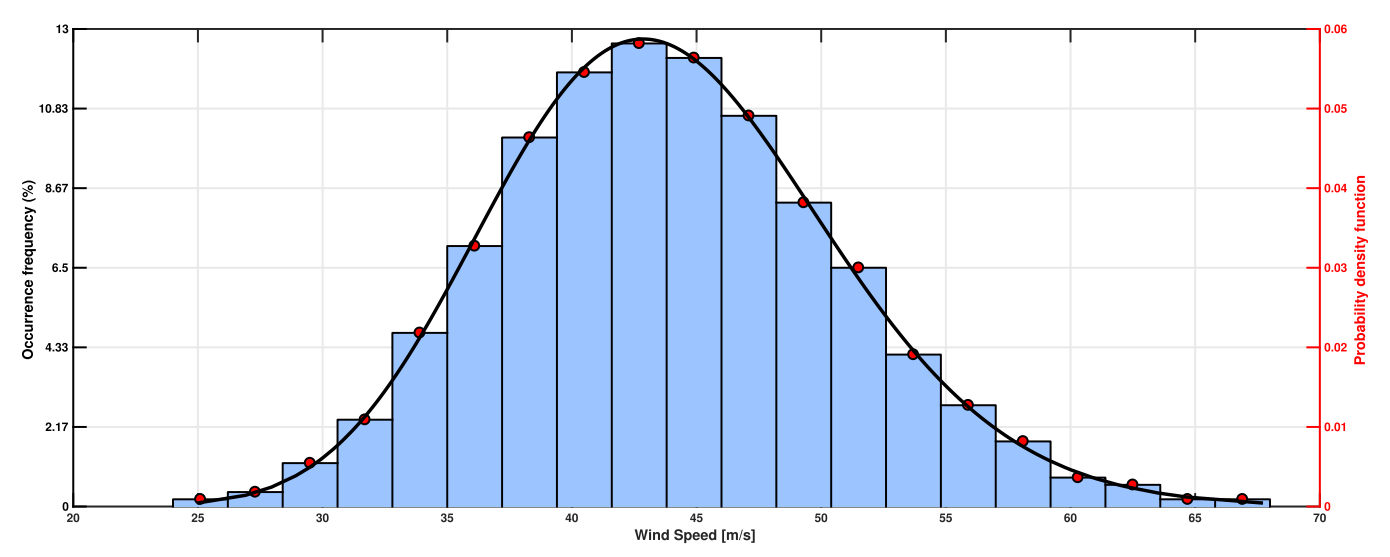


Fig. 4. Design gust wind speed Gamma distribution vs occurrence frequencies obtained with LHS sampling techniques for 500 samples.

where f(t) is a realization for the simulation of  $f_0(t)$ ;  $\Phi_n$  is an independent random phase angle in the interval  $[0-2\pi]$ ; N is an integer number that defines the discretization of  $S^0(\omega)$  in the frequency domain; and  $\omega_n$  represents an upper cutoff frequency for the spectral density function, calculated as  $n\Delta\omega$ , that represents the threshold over which the  $S^0$  function become negligible for either mathematical or physical reasons. This simulation is a periodic function with a period equal to

$$T_0 = nV \frac{2\pi}{\Delta\omega} \tag{3}$$

where nV is equal to 1 for the 1D-1V case. When the simulation is conducted over this period of time, the spectral density function of the realization  $S(\omega)$  is equal to that of the stochastic process. Simulating a time interval less that  $T_0$  instead will lead to small errors between the simulated and the target spectral density.

Eq. (2) can be adapted to simulate the along-wind fluctuation occurring at multiple points. In this case, a one-dimensional n variable (1d-nV) stochastic process must be simulated to account for the spatial correlation of wind velocities in a wind field. Hence, the simulated process  $f_0(t) = [f_{0,1}(t), ..., f_{0,n}(t)]$  is defined by a cross-spectral density matrix  $\mathbf{S}^0(\omega)$ , in which the diagonal terms are power spectral density functions and the off-diagonal terms are cross-spectral density functions.

It can be shown that the cross-spectral density matrix is non-negative definite [32], hence the Cholesky decomposition can be applied to find a matrix  $\mathbf{H}(\omega)$  such that

$$\mathbf{S}^{0}(\omega) = \mathbf{H}(\omega)(\mathbf{H}^{*}(\omega))^{\mathrm{T}}$$
(4)

where the symbol  $(\cdot)^*$  denotes the complex conjugate operation, and the superscript T indicates the transpose process. The matrix  $\mathbf{H}$  is a lower triangular matrix whose entries are complex numbers defined by their magnitude,  $|H_{ij}(\omega)|$ , and phase,  $\theta_{ij}(\omega)$ , where i and j are integers spanning from 1 to nV.

Using elements of the  $H(\omega)$  matrix, one can write Eq. (2) in the following more efficient form:

$$f_k = 2 \sum_{q=1}^{nV} \sum_{p=1}^{N} |H_{qp}(\omega)| \sqrt{\Delta \omega} \cos \left[\omega_{qp} t - \theta_{qp}(\omega_{qp}) + \Phi_{qp}\right] \text{ with } k$$

$$= 1, 2, \dots, nV$$
(5)

$$\omega_{qp} = p\Delta\omega - \frac{nV - q}{nV}\Delta\omega \tag{6}$$

While this formulation of the simulation is more efficient, the computational cost is still high, especially as nV increases. To overcome this high computational cost, Deodatis [33] proposed the use of the fast Fourier transform (FFT) to calculate the realization of the stochastic process. With this approach, Eq. (5) can be written as a function of specific coefficients defined as

$$B_{ksl} = 2 |H_{ks}(\omega_{sl})| \sqrt{\Delta \omega} e^{[-i\theta_{ks}(\omega_{sl})]} e^{[i\phi_{sl}]}$$
(7)

$$\omega_{sl} = l\Delta\omega - \frac{s}{nV}\Delta\omega \tag{8}$$

where p = 1,2,...,(nV)M-1; k = 1,2,...,nV; l = 0,1,...,M-1; and M is a integer number correlated to the chosen time step  $\Delta t$  and number of frequency discretization, N:

$$M\Delta t = \frac{2N\pi}{\omega_n} \tag{9}$$

Hence, the choice of M is not independent from N. In order to avoid aliasing in the simulation, the following condition must be imposed:

$$\Delta t \le \frac{2\pi}{2\omega_n} \tag{10}$$

Combining Eq. (10) with Eq. (9), the following relationship between M and N can be found:

$$M \ge 2N \tag{11}$$

where M must be a power of two to enable an inverse FFT to be used on the summation of the B coefficients.

In this study, the FFT approach is implemented by defining both the diagonal and off-diagonal terms of the cross-spectral density matrix  $S^0(\omega)$  for the along-wind fluctuation. The diagonal terms are defined using the model proposed by Kaimal et al. [34]:

$$S_{mm}^{0}(z_{m},\omega) = \frac{1}{2} \frac{200}{2\pi} u_{*}^{2} \frac{z_{m}}{\bar{\mathbf{U}}(z_{m})} \frac{1}{\left[1 + 50 \frac{\omega z_{m}}{2\pi \bar{\mathbf{U}}(z_{m})}\right]^{5/3}}$$
(12)

where  $z_m$  is the height of the  $m^{\text{th}}$  point (m),  $\bar{U}(z_m)$  is the mean wind speed at  $z_m$  (m/s), and  $u_*$  is the shear velocity of the flow (m/s) (Eq. (17)).

On the other hand, the off-diagonal terms are defined using the model proposed by Davenport [35] for the coherence function  $\gamma$  (Eqs. (13) and (14)):

$$S_{mn}^{0}(z,\omega) = \sqrt{S_{mm}^{0}(z_{m},\omega)S_{nn}^{0}(z_{n},\omega)}\gamma_{mn}(\Delta z,\omega)$$
(13)

$$\gamma_{mn}(\Delta z, \omega) = \exp\left[-\frac{\omega}{2\pi} \frac{C_z |z_m - z_n|}{\frac{1}{2} [\bar{\mathbf{U}}(z_m) + \bar{\mathbf{U}}(z_n)]}\right]$$
(14)

where the subscripts m and n indicate quantities for the  $m^{\text{th}}$  and the  $n^{\text{th}}$  point, respectively; z is the height of the point (m);  $\bar{U}$  is the mean hourly wind speed at height z (m/s); and  $C_z$  is an empirical adimensional constant that, for design purposes, can be assumed to be equal to 10 [36]. Note that the coherence between the poles is not considered in this study due to the significance distance between the poles (30.48 m, as per Section 4.2), which makes the wind speeds at the poles practically uncorrelated.

It must be noted that Eqs. (12)–(14) use the mean wind speed to define the power spectral density at a given point. However, the samples drawn from the PDF are representative of the 3-second gust peak wind speeds. To account for this difference, a conversion between the wind speed averaging times is needed. This study implements the following equation from Simiu and Scanlan [36] for this purpose:

$$\bar{\mathbf{U}}(z_{10}) = U_3 \left( \frac{2.5 \ln(z_{10}/z_0)}{2.5 \ln(z_{10}/z_0) + \beta^{1/2} c(t)} \right)$$
(15)

where  $\bar{\mathbf{U}}(z_{10})$  is the mean hourly wind speed at 10 m height;  $U_3$  is the 3-second gust wind speed obtained from the statistical analysis;  $z_{10}$  is equal to 10 m;  $z_0$  is the roughness length (m), which is a characteristic of the site terrain;  $\beta$  is an adimensional parameter function of  $z_0$ ; and c (t) is a coefficient obtained from statistical studies on wind records [36]. For this study, both parameters  $z_0$  and  $\beta$  are chosen to represent the condition of open terrain, with values of 0.07 m and 6.0, respectively [36]. Since the samples model the 3-second gust wind speed, the coefficient c(t) is chosen to be equal to 2.85 based on Simiu and Scanlan's indications [36].

The conversion from the 3-second gust to a mean hourly wind speed alone is not sufficient to enable the use of Eqs. (12)–(14). A closer analysis of these equations highlights the mean wind speed dependence on the height. Since the conversion of Eq. (15) yields only the mean hourly wind speed at 10 m height, the logarithmic law presented in Simiu and Scanlan [36] is used to convert the mean wind speed from a height of 10 m to the various heights along the length of the pole:

$$\bar{\mathbf{U}}(z) = 2.5u_* \ln \left( \frac{z}{z_0} \right) \tag{16}$$

where U(z) is the mean hourly wind speed at height z (m/s), and  $u_*$  is the shear flow velocity (m/s) that is also a characteristic of the site. Its value can be evaluated from a known mean hourly wind speed at a given height. Since the mean wind speed at  $z_{10} = 10$  m is known, it is possible to evaluate  $u_*$  using the following relationship:

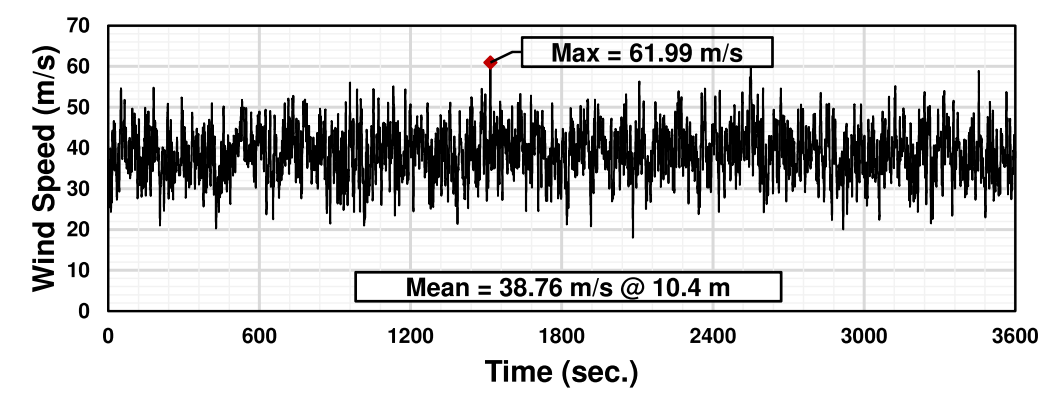


Fig. 5. Time history of one realization for target mean speed of 38.76 m/sec at 10.4 m height (tip of the pole).

$$u_* = \frac{\bar{U}(z_{10})}{2.5\ln\left(\frac{z_{10}}{z_0}\right)} \tag{17}$$

For this study, the pole was divided into seven segments where the wind loading is applied; therefore, the number of variables in the stochastic process nV is equal to 7. Applying the simulation method described in Eq. (5) combined with the wind velocity conversion laws in Eqs. (15) and (16), the wind velocity time histories are obtained at locations along the pole for each one of the 500 mean wind speeds, considering a wind event duration of one hour. Fig. 5 shows a realization of the wind speed time history with target mean wind speed of  $38.76 \, \text{m/s}$  at the tip of the pole, obtained with a time step of  $0.05 \, \text{s}$ .

To assess the accuracy of the simulation, the theoretical power spectral density (PSD) and the PSD obtained from the realizations are compared. Fig. 6 illustrates this comparison, where the PSD for the time history is computed using the Welch periodogram method [37]. The computed PSD shows good agreement with the theoretical value; hence, the wind simulation results are a good representation of the along-wind speed fluctuations. An additional step is required to convert the wind speed time histories to actual load time histories that can be applied to the distribution system. For this purpose, the equation proposed by Simiu and Scanlan [36] is used:

$$F_D = \frac{1}{2}\rho \bar{U}^2 C_D DL \tag{18}$$

where  $\rho$  is the air density at 15 °C (kg/m³),  $C_D$  is the drag coefficient, D is the diameter of the pole or conductor (m), and L is the length of the effective area (m). The drag coefficient is an adimensional number that depends on the shape of the section exposed to the wind. Therefore, since both the pole and the conductors have circular sections,  $C_D$  was set to 1.2 [36]. For the diameter of the conductor, the increment in radial thickness defined in the ice hazard section is used in Eq. (18) to

account for the additional forces induced in the system.

## 4. Vulnerability analysis

The 500 wind load time history samples generated in the previous section are used in a vulnerability analysis of the system. This analysis is conducted through the generation of fragility curves representing the probability of system failure. For this study, the failure criterion corresponds to an excess of the bending moment demand with respect to the nominal bending moment capacity of the distribution pole—a mode of failure that has been often observed in the field. This criterion accounts for both hazards, since the wind force relates to the ice-induced increment of the radial thickness of the conductor. However, for a comprehensive analysis of the system vulnerability, is also important to include the effect of aging on the pole's mechanical characteristics. The following subsections will present in detail each step required for the vulnerability analysis.

## 4.1. Pole properties

Distributions systems are built using various sizes and classes of distribution poles based on their availability. According to ANSI O5.1 [38], distribution poles are classified by the horizontal load capacity 61 cm below the tip of the pole. In this study, 12.19 m poles made from Southern Yellow Pine from classes 1 to 4 are considered as a component of the simulated system, and they are characterized by a horizontal capacity of 20.02 kN, 16.50 kN, 13.30 kN, and 10.68 kN, respectively (annex B of ANSI O5.1 [38]). These categories specify a minimum requirement for the circumference of the poles at the top and at 1.83 m from the bottom. Using these data, it is possible to evaluate the minimum requirement for the diameter of the poles at both locations. Therefore, the minimum required diameters at the top for each class are

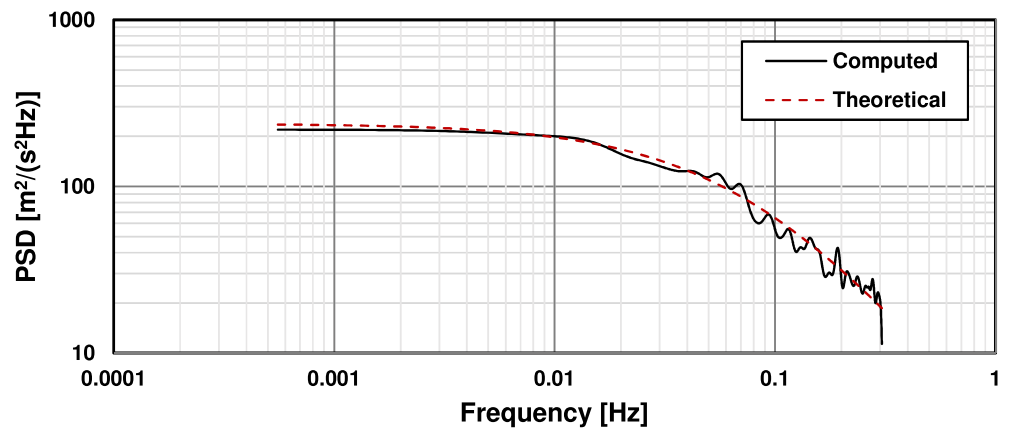


Fig. 6. Comparison of the theoretical and simulated power density functions for the wind events.

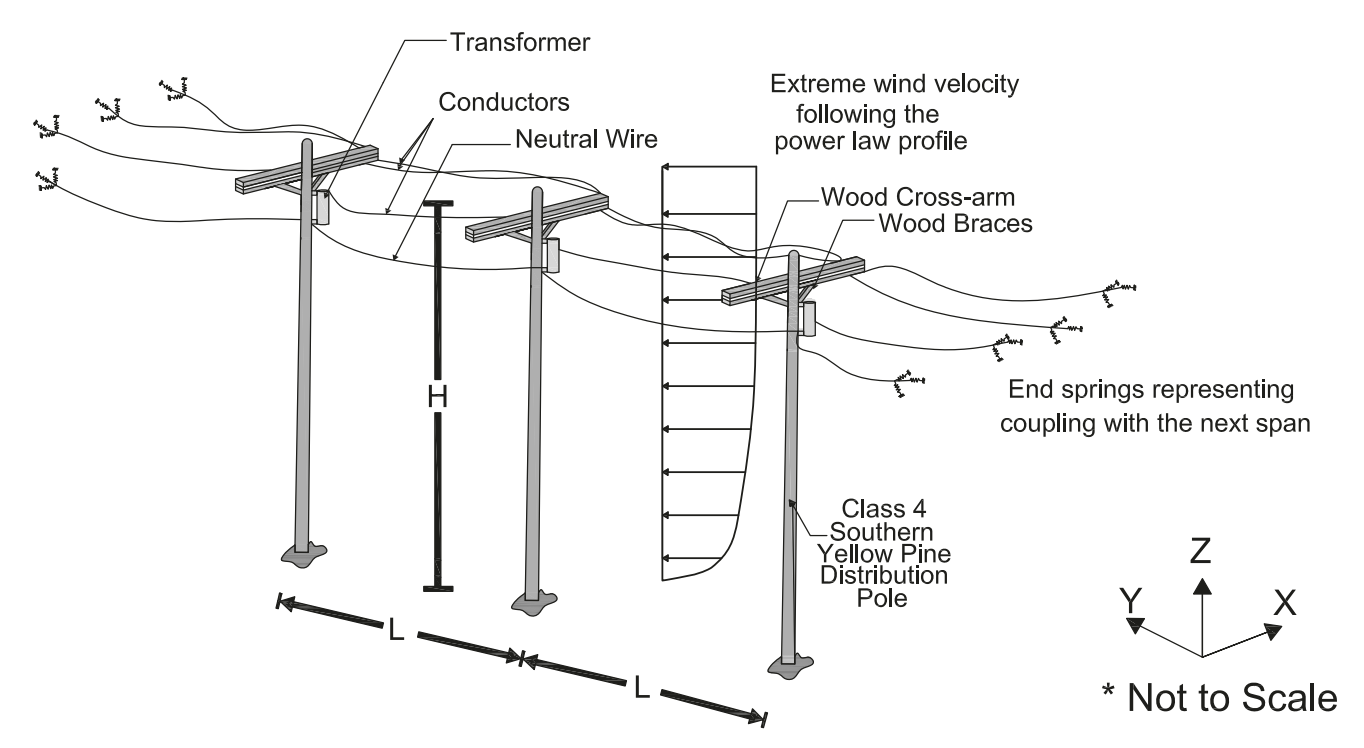


Fig. 7. Schematic model of the simulated power distribution segment with end springs in the FEM.

0.218, 0.202, 0.186, and  $0.170\,\mathrm{m}$ , respectively, and the minimum required diameters  $1.83\,\mathrm{m}$  from the bottom for each class are 0.331, 0.311, 0.291, and  $0.271\,\mathrm{m}$ , respectively. These diameter values are later used in the simulation of the poles in each class in the analyzed system. The same ANSI O5.1 standard, Table C.1, also indicates the values of the moment of elasticity to be used for each type of wood, which for the Southern Yellow Pine is equal to  $18.48\,\mathrm{GPa}$ .

## 4.2. System model

The system modeled in this study is composed of a set of three poles and the relative cables sagging between them (Fig. 7). This option is preferred over a single pole simulation as it accounts for the actual effect of the wind on the long span of the cables. The poles used in this system have a height of 12.19 m, of which 10.36 m are above ground while the remaining 1.83 m are buried underground, per ANSI O5.3 [39], and they are assumed to have a fixed boundary condition. Each pole is modeled using a single elastic tapered element to account for the variation in section between the groundline and the tip of the pole. Additionally, a combination of a cross-arm and braces is defined at 0.457 m below the pole tip to account for the portion of the system devoted to the connection with the cables. These additional elements are dimensioned according to ANSI O5.3 [39]; thus, there are rectangular cross sections for both components with dimensions of  $0.095 \times 0.070 \,\mathrm{m}^2$  and  $0.095 \times 0.146 \,\mathrm{m}^2$ , respectively. These components are modeled with single elastic elements using the same wood properties defined for the poles. The three poles are placed at a relative distance of 30.48 m, corresponding to the wind span of the cables. The conductors and the neutral wire are modeled using cables 336 ACSR 18/1 with a diameter of 17.4 mm and #4/0 ACSR 6/1 with a diameter of 14.3 mm, respectively.

For this type of simulation, Yang and Hong [40] suggested representing the effect of the span adjacent to the external poles using end springs with equivalent stiffness. Therefore, at both ends of the connectors and the neutral wire, end springs are defined to represent the coupling with the next span, as illustrated in Fig. 6 [41]. The value of the end-springs constant is obtained following the recommendation of Yang and Hong [40], using Eq. (19), which resulted in a value of

1751.30 N/m:

$$\frac{1}{K_{st}} = \frac{L_e}{AE} + \frac{q_y^2 L^3}{12T_o^3} \text{ and } L_e = L \times (1 + 8 \times S_L^2)$$
 (19)

where  $K_{st}$  is the stiffness of the end spring (N/m),  $L_e$  is the effective conductor length, A is the conductor cross-sectional area (m²), E is the conductor's elastic modulus (N/m²), E0, is the conductor's gravity distributed load (N/m), E1 is the span length between poles (m), E1 is the conductor's horizontal initial static tension force (N), and E2 is the sagto-span ratio.

This model is used to conduct a linear modal history analysis, applying the generated wind force time history to the whole system. For the poles, due to their tapered nature, the load is applied at 7 locations along the pole length, as shown in Fig. 8. The loads on the pole are obtained using Eq. (18), with L representing the average tributary length of each segment. The wind load on the conductor is determined using Eq. (18), considering the increment in diameter due to ice loading. This increment, for the Chicago area, corresponds to an additional thickness of 12.70 mm around the conductors and neutral wire.

#### 4.3. Moment capacity and aging mechanism

In order to build the fragility curve of the system, it is necessary to define a failure criterion for the distribution pole. In this study, the nominal bending moment capacity of the pole is used to assess the possible failure of the system under wind loading. Its value is determined based on the ultimate resisting moment formulation proposed by Elliot [42]:

$$M_{ult} = S_f K_r F_b C_g^3 (20)$$

where  $S_f$  is the NESC strength factor (considered equal to 1.0 to represent the nominal bending capacity in this study),  $K_r$  is the calculation constant of 0.003168,  $F_b$  is the wood fiber strength equal to 55200 kPa for Southern Yellow Pine, and  $C_g$  is the groundline circumference of the pole (m).

The failure criterion of the system is defined as the instant when the maximum wind-induced bending moment exceeds the defined

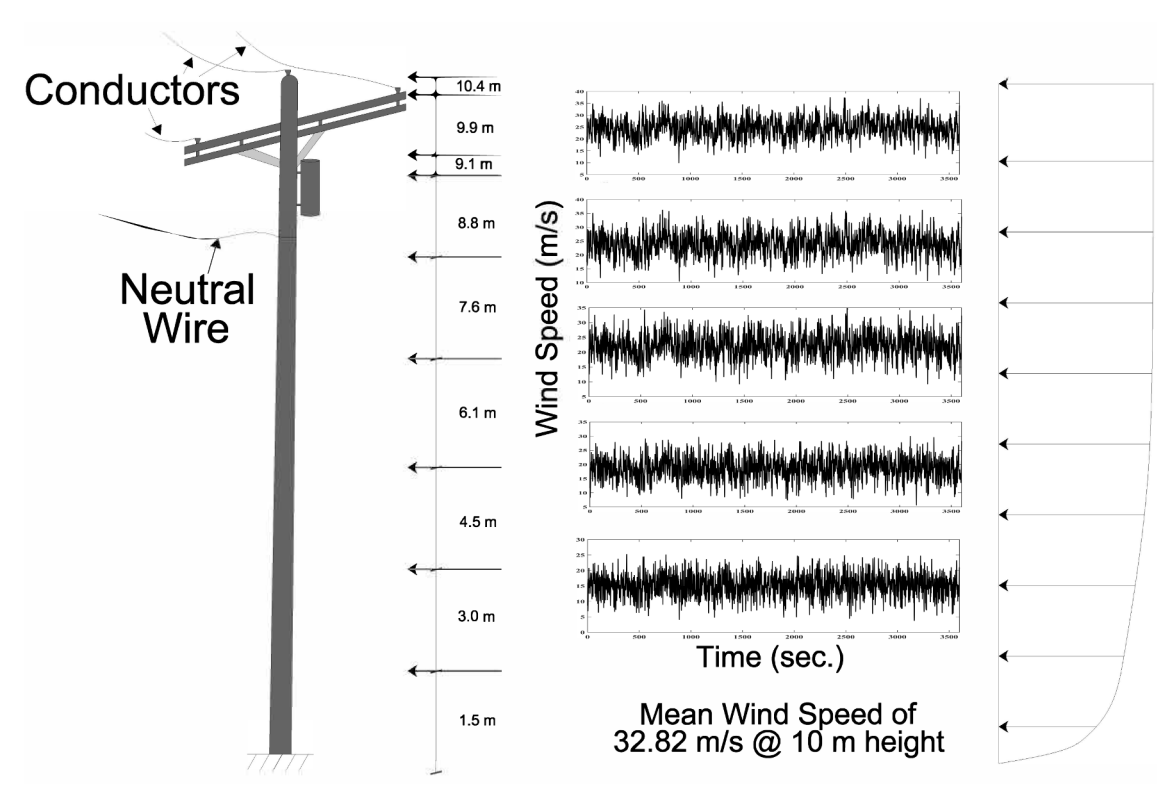


Fig. 8. The location of the wind load acting on the poles with the wind speed time history realizations at different heights for target mean speed of 32.82 m/sec. at 10 m height.

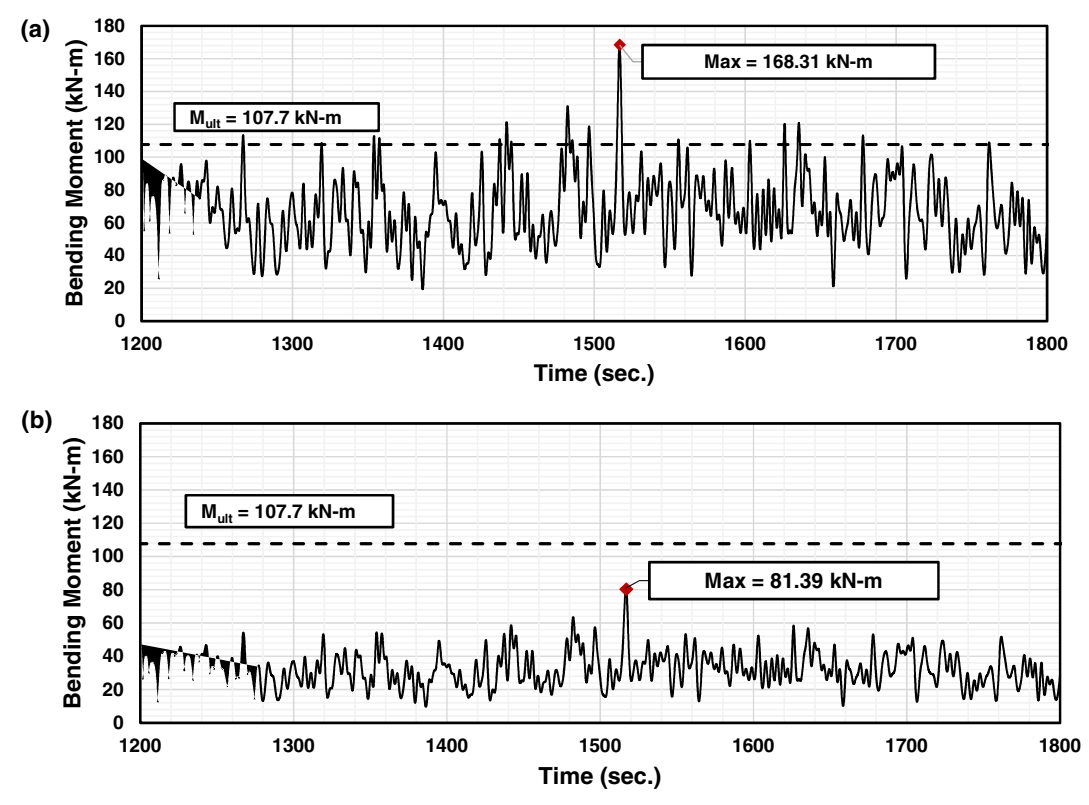


Fig. 9. Two independent samples of the random bending moment time history at the base of the pole for both conditions, (a) with ice and (b) without ice on the conductors and neutral wire. Both samples correspond to the wind crossing with mean speed of 38.76 m/sec. at 10.4 m height that corresponds to the time histories shown in Fig. 5.

threshold, which is the nominal bending moment capacity defined by Eq. (20). The application of this criterion is shown in two examples of the wind-induced bending moment at groundline in Fig. 8. In this figure, the horizontal dashed line represents the threshold moment capacity of the class 1 pole, while the circles indicate the threshold crossing for the target mean wind speed of 38.61 m/s. This point in time is considered a failure event for the pole, and it will be used as the base information for the construction of the fragility curves. It also noticeable that, while a failure event occurs when the ice hazard is considered (Fig. 9a), the case without the additional ice thickness does not show any sign of failure under this wind realization (Fig. 9b).

To fully analyze the power distribution poles, one must also study the effect of aging mechanisms on strength degradation and loss of cross section [1]. These mechanism are induced by several causes, such as fungal decay, surface rot, fatigue, and insect infestation [43,44]. Among these, fungal growth is particularly relevant for wooden structures due to the organic nature of wood [45] and the direct contact of the pole with the ground. In fact, power poles are typically buried 1.83 m underground to create the necessary strength capacity to hold the wood pole in place. This buried portion is in direct contact with the soil, becoming an ideal environment for the growth of fungi. The presence of fungi will cause the wood to decay by breaking down the wood fibers and reducing the effective diameter and thus the nominal moment capacity of the pole [46]. Also, depending on the moisture content of the soil and the possible presence of chemicals, there is the possibility of an increase in the rate of fungal decay [47]. The decayed portion of the wood poles will also attract an insect infestation [43], such as by termites or other insects that may damage or feed on the wood. Approximately 85% of the distribution poles inspected by the Rural Utilities Service (RUS) are made of thick sapwood Southern Pine [48], which is more prone to decay and insect infestation due to moisture content promoting fungi growth. For these reasons, it is important to include both the probability and the effect of such decay in the analysis. In regard to the probability of decay for a given pole, Li et al. [49] observed a sample of 13,940 wooden distribution poles in the field, with ages ranging from 1 to 79 years, and found that 8% of poles are undergoing decay. Based on these observations, they proposed a linear model for the decay probability of a given pole,  $P_D(t)$ , as a function of its age in years, t:

$$P_D(t) = \begin{cases} 0 & \text{if } t \le 0\\ 0.004t - 0.04 & \text{if } t > 10 \end{cases}$$
 (21)

Once decay is detected in a pole, it is possible to estimate its depth at time t,  $d_t$  (mm), using the model proposed by Wang et al. [50] and Bjarnadottir et al. [46]:

$$d_{t} = \begin{cases} ct^{2} \\ (t - t_{lag})r \end{cases} \begin{cases} if & t \le t_{d_{0}} \\ if & t > t_{d_{0}} \end{cases}$$
(22)

$$t_{lag} = 3r^{-0.4} (23)$$

$$r = k_{wood} k_{climate} (24)$$

$$t_{d_0} = t_{lag} + \frac{d_0}{r} \tag{25}$$

$$c = \frac{d_0}{t_{co}^2} \tag{26}$$

where c is the decay coefficient,  $t_{\rm lag}$  is the decay time lag (years),  $t_{\rm do}$  is the time of decay (years), r is the decay rate (mm/year),  $k_{\rm wood}$  is the wood parameter,  $k_{\rm climate}$  is the climate parameter, and  $d_{\rm o}$  is the initial decay depth. Since there are no data available for the initial decay depth, it is assumed to be 5 mm [50].

As discussed earlier, the decay process will reduce the effective diameter of the pole. Therefore, an updated threshold value of the bending moment can be calculated by substituting the effective diameter of the decayed pole for the original diameter in Eq. (20). To evaluate the new diameter through Eqs. (22)–(26), it is necessary to evaluate the wood and climate parameters. The findings of Bjarnadottir et al. [46] for Southern Pine timber poles indicate a wood parameter value of 0.38. The method proposed by Wang et al. [50] can be used to estimate the climate parameter as a function of the mean annual temperature, rainfall, and number of dry months. The proposed equations for this method are

$$k_{climate} = f(R_{mean})^{0.3} f(T_{mean})^{0.2}$$
 (27)

$$\begin{cases}
R_{mean} = \begin{cases}
0 \\
f_0(R_{mean})(1 - \frac{N_{dm}}{6})
\end{cases} & \text{if } R_{mean} \le 250 \text{ mm or } N_{dm} > 6. \\
\text{if } R_{mean} > 250 \text{ mm and } 0 \le N_{dm} \le 6.
\end{cases}$$
(28)

$$f_0(R_{mean}) = 10[1 - e^{-0.001(R_{mean} - 250)}]$$
(29)

$$f(T_{mean}) = \begin{cases} 0 & \text{if } \leq 5^{\circ}C \\ -1 + 0.2T_{mean} \\ -25 + 1.4T_{mean} & \text{if } \leq 5^{\circ}C \\ \text{if } 5 < T_{mean} \leq 20^{\circ}C \\ \text{if } T_{mean} > 20^{\circ}C. \end{cases}$$
(30)

where  $R_{\rm mean}$  is the average annual rainfall (mm),  $T_{\rm mean}$  is the average annual temperature (°C), and  $N_{\rm dm}$  is the number of dry months annually (month).

This study is in the Midwest (Chicago area), where there are typically no dry months in any year. The average annual rainfall and the average annual temperature are 843 mm and 9.8  $^{\circ}$ C, respectively. Based on this information, the climate parameter and the decay rate are determined to be 1.53 and 0.58 mm/year, respectively. Due to the high demand on distribution poles, the class 1 pole size is used to represent the effects of decayed poles. The decay depth and the moment threshold at various times are shown in Table 2.

## 4.4. Fragility curves

To assess the reliability of the distribution poles, fragility functions are developed to determine the probability that critical engineering demand parameters of the structure exceed certain limit states for a given hazard intensity. For wood poles, the engineering demand parameter of interest is the nominal resisting moment capacity; the considered limit state is failure of the pole, which is defined as the demand moment exceeding the capacity; and the hazard intensity is the wind speed. Therefore, the limit state function used for the fragility analysis is defined as follows:

$$Z(t) = M_{ult}(t) - M(t)$$
(31)

where  $M_{ult}(t)$  is the nominal bending moment at any time t (kN-m) representing the pristine or decayed states of the poles, and M(t) is the moment demand at the groundline of the pole (kN-m). By analyzing this limit state function, it is possible to obtain temporal data indicating when and if failure occurs for each one of the simulated wind velocities and class poles. Fig. 10 shows the results of this analysis that represent the maximum bending moment against the relative average wind speed for class 1 poles, with and without the effect of ice hazard. Here, failure for a given wind speed is visualized as the crossing of the collected data with the nominal bending moment value (shown as a dotted red line). Notice that, similarly to that observed in Fig. 9, the ice condition

**Table 2**Decay depth and ultimate moment threshold at various times, *t* for Class 1 pole.

Time, t (years)	0	25	50	75
Decay Depth, $d_t$ (mm)	0.00	12.37	26.90	41.44
Effective Decayed Diameter, $D_{de}$ (mm)	331.49	319.12	304.58	290.05
Ultimate Moment Threshold, $M_{ult}$ (kN-m)	197.50	176.21	153.21	132.31

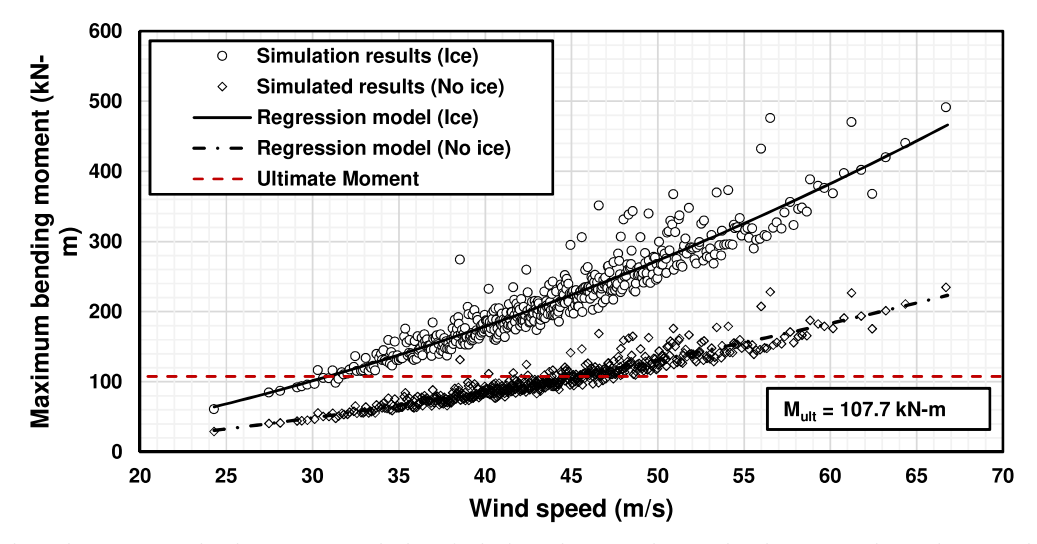


Fig. 10. Wind speed vs. maximum bending moment at the base for both conditions, with ice and without ice on the conductors and neutral wire.

induces failures in the pole at a significantly lower wind speed than failures occurring in the absence of ice. This confirms that winter blizzards can cause damage to the distribution system even for more frequent events.

From these data, fragility curves are developed using a log-normal distribution function to fit the results. The cumulative distribution function (CDF) function is given by:

$$p = \frac{1}{\sigma\sqrt{2\pi}} \int_0^{v_{max}} \frac{e^{\frac{-(\ln(v) - \mu)^2}{2\sigma^2}}}{v} dv$$
 (32)

where p is the cumulative probability that the moment capacity is exceeded,  $\mu$  is the location parameter (log mean) (m/s),  $\sigma$  is the scale parameter (log standard deviation) (m/s),  $\nu$  is the mean wind speed (m/s), and  $\nu_{max}$  is the maximum wind speed (m/s).

The location and scale parameters of the fragility curve are estimated using the maximum likelihood method [51]. Fig. 11 shows the fragility curves for all four classes of poles analyzed in this study. Additionally, the effects of decay at different times for the class 1 poles are shown. Here, the pristine curves of class 1 and class 4 are used as boundary limits to highlight the extent of the decay effect on the failure probability.

## 5. Impact of hazard mitigation strategies

There are many strategies to harden distribution poles against wind load, each with advantages, disadvantages, additional costs, and

interrelationships with other approaches [52]. These approaches include: (i) stronger poles, such as steel or composite (concrete is too heavy for the typical digger derrick trucks); (ii) a steel brace that is driven below the groundline and extends above the third-party attachments (guyed poles) or, alternatively, fiberglass wraps; (iii) shorter spans, which require more poles per line distance of distribution lines; (iv) reduced conductor size, which directly reduces the load on the pole but impacts the electric capacity of the line; (v) reduced pole-mounted equipment, achieved by converting a three-phase pole-mounted transformer bank to a pad-mount unit; (vi) underground placement of the conductors when possible, which increases the cost per mile of line; and (vii) fewer third-party attachments.

This study specifically focuses on two commonly used approaches to mitigate the hazards of wooden power poles: guyed poles and larger poles. Using a guy cable, distribution poles can withstand and resist higher wind loads and will experience reduced deformation, as part of the shear forces and bending moments are transferred to the ground through the guy cable. Since the cables are pretensioned, they are modeled with the maximum initial unloaded tension of 35% of the rated breaking strength (RBS), as specified in ASCE 74 [53]. One important aspect is the guy lead. Improper placement of the guy attachment and anchor will cause problems such as pole buckling due to a short guy lead. The ratio of the guy lead to the guy attachment height will determine the amount of tension that can be carried by the guy cable. Fig. 12 shows a schematic model of the pole system, with the guy cable and the possible variations in the lead. Shorter guy leads will cause the guy cable to carry more tension.

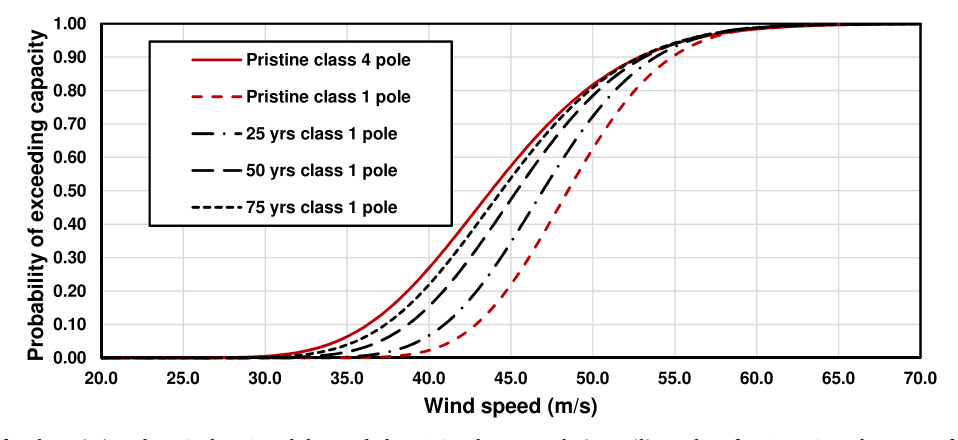


Fig. 11. Fragility curves for the pristine class 4, class 1 and decayed class 1 Southern wood pine utility poles after 25, 50, and 75 years for combined ice and wind loading condition.

Fig. 12. The guyed pole system and the impact of different lead angles on the tensile force in the cable.

Due to the high tension along the z-axis, the guy cable will exert axial forces in the distribution pole that could increase the likelihood of a buckling failure. High tension in the cable could also cause tension failure or anchor pull-out failure of the guy cable. On the other hand, a longer guy lead will require more right-of-way that could cause safety issues with the public. Therefore, a ratio of 1:1 for the guy lead and a guy attachment height with 45° angles are used to model the guyed distribution pole. A 12.7 mm diameter, tension-only, high-strength galvanized steel strand with a rated breaking strength (RBS) of 83.63 kN was selected as the guy cable. The material and section properties are obtained from USSC [54] and Union [55]. Guv cables consist of turnbuckles to tighten the wire, and different types of anchors are used to attach the guy cable to the ground. Other components of the guy cables are assumed to be installed perfectly without experiencing any failures before flexural or tension failure of the pole and guy cable. Based on ASCE 91 [56], the maximum allowable tension of the guy cable is limited to 65% of the RBS to prevent the guy cable from reaching the yield point. Therefore, 54.36 kN will be used as the maximum allowable tension.

By installing a guy cable, a hinge support is added at the height of the guy attachment. This causes the bending moment to be reduced at the base of the pole. To assess the failure of the guyed distribution poles, the simulated wind load histories are applied to the pole-guy-conductor system. The maximum bending moment of the pole at groundline and the maximum tension of the guy cable obtained from FEM results are shown in Fig. 13. In this case, the maximum value of the bending moment and the guy cable tension experienced by the system are 10.23 kN-m and 78.34 kN, respectively. These results show a significant improvement in bending moment demand reduction, which helps prevent flexural failure at the base of the pole. On the other hand,

the maximum tension of the guy cable is more than the 65% RBS of 54.36 kN, which makes the cable prone to yielding. Therefore, in this study, the maximum tension demand of the guy cable was used as the limit state function for the fragility analysis under the applied wind load. However, it is important to note that, in actual situations, this is not the only failure mode that should considered when designing for the guy cable. For example, failures could happen if the installation of the guy component is not satisfactory or if trees fall on the guy cable, which will increase the tension on the guy cable.

The fragility curves for a pristine pole, with and without the guy, are illustrated in Fig. 14, and their analysis shows a significant decrease in the vulnerability of the distribution poles due to the addition of the guy cable. However, this mitigation method does not consider the effect of wind from the other direction. Guy cables are not meant to withstand any compression force. Thus, the direction of the prevalent wind must be considered when designing this mitigation method for the most efficiency. This mitigation method can be further enhanced by adding more guy poles in different directions or by using a larger-diameter or extra high-strength galvanized steel strand.

Another mitigation method is the use of a stronger distribution pole from a higher pole class size. Based on ANSI O5.1 [38], the minimum circumference at 1.83 m from the pole base for class 1, class 2, and class 3 poles made from 12.2 m Southern Pine are 1.04, 0.98, and 0.91 m, respectively. As shown in Eq. (20), to calculate the nominal resisting moment, the groundline circumference of the pole has an exponent value of 3. Thus, a slight increase in the pole groundline circumference will increase the bending moment capacity notably. Fig. 15 shows that upgrading from a class 4 to a class 2 can result in decreasing the probability of failure from 30% to 10% under a wind speed of 40 m/sec. However, this solution is not always practical, as it requires complete

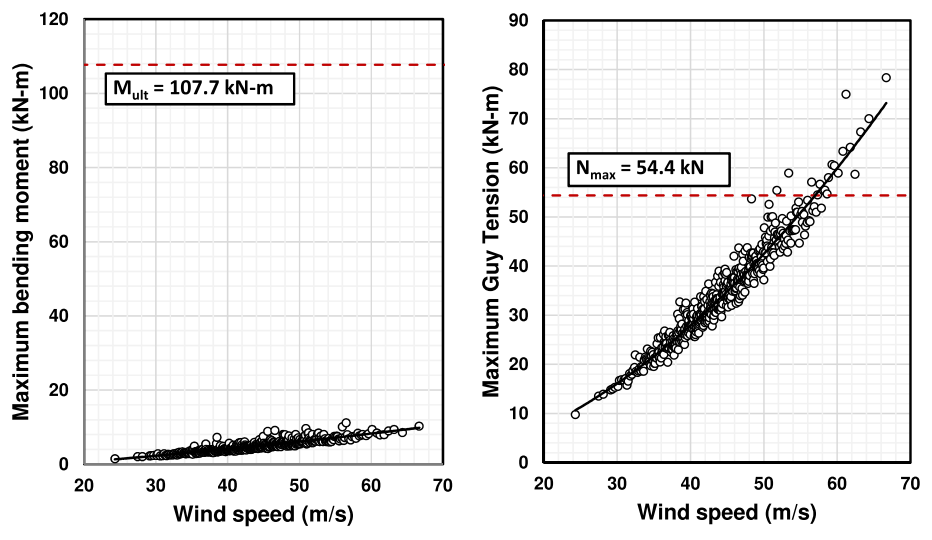


Fig. 13. (a) Wind speed vs. maximum bending moment at the base. (b) Wind speed vs. maximum guy tension.

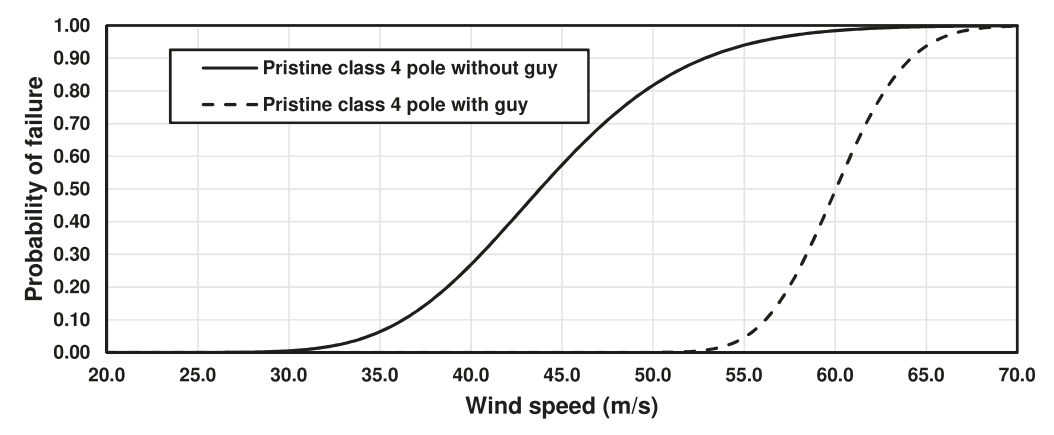


Fig. 14. Fragility curves for class 4 Southern wood pine utility poles with and without guy.

replacement of existing poles with larger poles that also have a higher initial cost. As observed, these strategies are efficient but present economic and technical problems that may limit their use. To make proper decisions on the implementation of these strategies, it is necessary to assess the return on investment of their application over the life of the structure. For this purpose, the next section presents a life-cycle cost analysis (LCCA) of these approaches to provide a rational tool for assessing and selecting a suitable approach for each case.

## 6. Life-Cycle Cost Analysis (LCCA)

To validate the practicality of the hazard mitigation strategies, an estimated 70 years of life-cycle cost assessment is performed for the poles with each of the mitigation strategies. According to the NESC [28], distribution poles are required to be replaced whenever their deterioration reduces their capacity by 1/3 of the pristine value. The deterioration can be determined during the inspection and maintenance of the poles. However, as mentioned above, due to the high demand of wind loads on the poles, class 4 poles are not suitable for representing the decay effect due to their low capacity. Therefore, in this study, the class 4 pole is assumed to be replaced if any sign of decay is detected during the inspection cycle. By performing LCCA, a framework can be developed to ensure the appropriate allocation of resources [57,58]. The life-cycle cost (LCC) is determined based on assumptions and a justification is made for the life cycle of a distribution pole. The LCC for a distribution pole includes the initial cost of material as well as installation, labor, and transportation costs. Inspection and maintenance will be required at a specified time interval. Failure of distribution poles can potentially cause several days of outages, which can result in a great amount of expense. Accounting for all of these contributions, the LCC is determined as

$$LCC = C_i + C_{I\&M} + C_f + C_{out} (33)$$

where  $C_i$  is the initial cost of the distribution poles,  $C_{\rm IRM}$  is the inspection and maintenance cost,  $C_{\rm f}$  is the failure cost, and  $C_{\rm out}$  is the outage cost. Details of each cost category are further explained in this section. It is important to note that the LCC calculation must be made on the time value of money for each of the cost items. To calculate the present value of future cost items, a discount factor, z, is used as shown in Eq. (34):

$$z(t) = (1+r)^{-t} (34)$$

where r is the discount rate. According to a FEMA recommendation [59], a discount rate of 4% is used in this study.

#### 6.1. Initial, inspection, and maintenance costs

The initial cost,  $C_{\rm i}$ , is a one-time cost incurred from purchasing, shipping and handling, and installation of the distribution pole and the guyed pole. The distribution pole costs include the wood pole, wood cross-arm and braces, and 30.5 m of conductor (which is the span length considered in this study). These costs are based on the current market price of wood poles from American Timber and Steel, conductor and neutral wires from Southwire, and guy cables from Valmont Site Pro 1. Other costs, such as cost of installation and transportation, are from allcostdata.com. For guyed distribution poles, the cost of the guy cable and the guy components are included in the initial material cost. Labor cost are considered in the installation cost.

The cost of inspection and maintenance are calculated based on the inspection cycles. This cost includes performing the inspection, applying any wood pole treatment to help retain the initial strength of the distribution poles and guy cable, and replacing a decayed pole. Two scenarios are considered for the inspection and maintenance costs. In

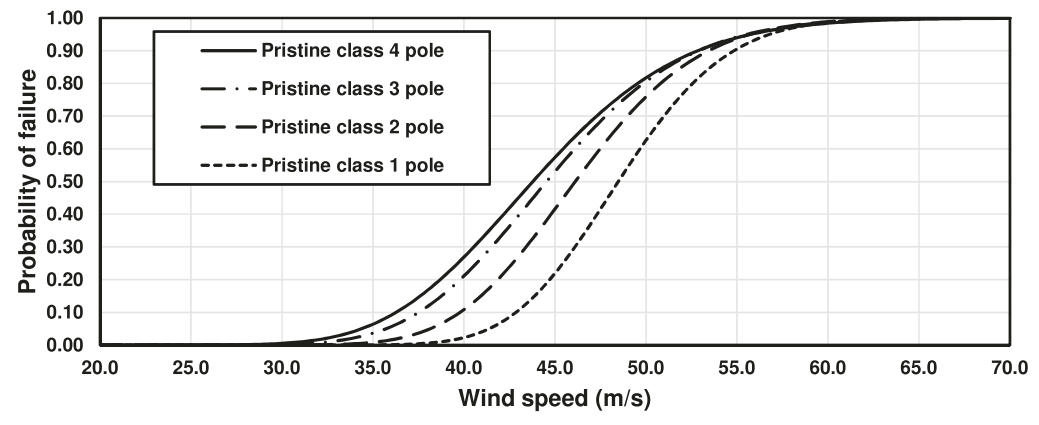
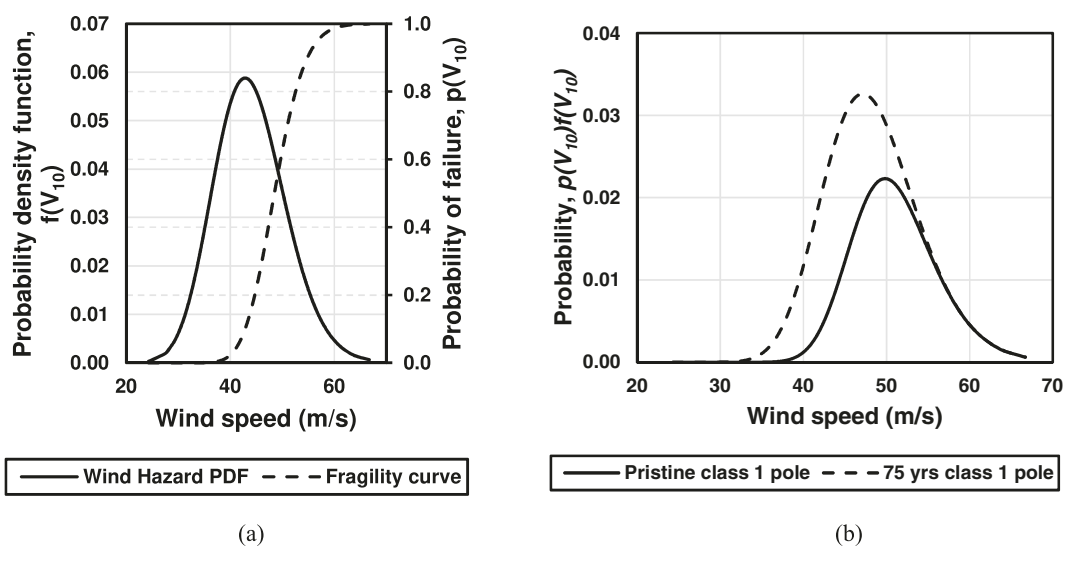


Fig. 15. Fragility curves for class 1 through 4 of the southern wood pine distribution poles.



**Fig. 16.** (a) Hazard curve,  $f(V_{10})$ , and the fragility curve,  $p(V_{10})$ , and (b) the convolution of the hazard and fragility curve,  $f(V_{10})$  for pristine Class 1 pole and 75 years decayed class 1 pole.

the first scenario (Case 1), the effects of decay are considered during the lifetime of the poles using the developed fragility curves. The second scenario (Case 2) assumes that the pole is fixed every time decay is observed at each maintenance inspection, to avoid further decay and to bring the pole back to pristine conditions. Vegetation management and wildlife protection costs are not included due to the limited availability of that information. Based on a survey of different utility companies by Mankowski et al. [60], distribution poles are typically inspected every eight years. The inspection and maintenance costs per pole are assumed to be \$280 per inspection [61]. A total of eight inspections are considered to be performed throughout the life cycle of the pole. The probability of decay at time *t* during each of the inspection cycles can be determined using Eq. (21). Combining all the illustrated terms, the total inspection and maintenance costs are determined by

$$C_{I\&M}(t) = \sum_{i=1}^{n} (M_{Z}(t) + C_{R,P}P_{D}(t))$$
(35)

where M is the inspection and maintenance cost, n is the number of inspections,  $C_{R,P}$  is the cost of pole replacement when decay is detected, and  $P_D(t)$  is the decay probability for the pole.

#### 6.2. Failure cost

The failure cost is the portion of the cost associated with the probability of pole failure. Its evaluation is based on using the fragility curves (defined in Section 4) combined with the estimated wind hazard level (defined in Section 2) to evaluate the failure-induced cost for a given period of time t. Therefore, the expected failure cost at time t can be defined as

$$C_{sf}(t) = \sum_{i=1}^{L} C_R z(t) P_f(t)$$
(36)

where L is the total number of load occurrences between time 0 and time t,  $C_R$  is the cost of replacement associated with failure, and  $P_f(t)$  is the probability of failure for the pole given the mean arrival rate of the considered hazard.

For the failure cost,  $C_R$ , the failed pole is considered irreparable, and a new pole is required. Therefore, the replacement cost of the pole includes the removal of the failed pole and the initial cost of the new pole. Additional cost items are considered for guyed distribution poles, including the cost of new guy cable and the guy components.

The number of events occurring until time t is treated as a Poisson

process with an average occurrence rate,  $\nu$ , that can be determined as suggested by Wei and Caracoglia [62]:

$$v = 1 - F_{zf} \tag{37}$$

where  $F_{xf}$  is the probability of the wind speed characterized by a non-zero fragility. Using the results from the previous section, this value is calculated to be  $\nu=1$ , which represents an average of at least one high-speed wind per year.

The probability of failure for the examined poles is described as a Poisson process using the equation described in Ierimonti et al. [63]:

$$P_f(t) = -\frac{1}{vt}log(1 - P_{tf})$$
(38)

where  $\nu$  is the mean arrival rate for the Poisson process defined above, and  $P_{\rm tf}$  is the failure probability at time t defined as

$$P_{tf} = 1 - [1 - P_{1f}]^t (39)$$

where  $P_{1f}$  is the annual probability of failure of the pole. This probability is determined as the convolution integral between the fragility and the hazard curves [62]:

$$P_{1f} = \int_0^\infty p(U(z_{10})) f(U(z_{10})) dU(z_{10})$$
(40)

where  $V_{10}$  indicates the reference wind speed at 10 m high,  $p(V_{10})$  is the fragility curve described in Eq. (32), and  $f(V_{10})$  is the hazard curve described by Eq. (1). The hazard curve, fragility curve, and the convolution of the function for both a pristine class 1 pole and a 75-year decayed class 1 pole are shown in Fig. 16.

The value of  $P_{1f}$  will be influenced by the decay process described in Section 4, due to the differences in the fragility curves for the various decay states. Therefore, to investigate the effects of decay and possible maintenance on the failure costs, two different scenarios are considered. In the first scenario, the decay is considered during the lifetime of the pole, using fragility curves interpolated from the ones already calculated. The second scenario instead considers that the pole is repaired at each maintenance inspection to avoid further decay and to bring the pole back to pristine condition. Fig. 16 illustrates the failure cost normalized to the initial cost for a decaying scenario for pole classes 1, 2, and 3 together with the guyed class 4 pole.

#### 6.3. Outage cost

Distribution poles are a crucial component in the distribution network, and each severe windstorm that leads to a failure is expected to

**Table 3**Estimated cost for each category for Case 2B (75% of total maintenance expenses).

Mitigation Cost for Case 2B	Class 3	Class 2	Class 1	Guyed
Initial Cost, $C_i$	\$1,971	\$2,012	\$2,076	\$2,277
Inspection/Maintenance Cost, $C_{I\&M}$	\$826	\$832	\$841	\$819
Failure Cost, $C_f$	\$5,423	\$4,580	\$3,342	\$331
Outage Cost, Cout	\$7,152	\$5,974	\$4,294	\$387
Total Life Cycle Cost	\$15,373	\$13,400	\$10,555	\$3,816

cause a power outage that may require two or more days for a complete fix. Based on the data available, any outage is assumed to cost 50% of the total maintenance expenses [64]. For this study, the sum of the inspection, maintenance, and replacement costs is considered to be the total maintenance expense. Due to the variation of outage costs between urban and rural areas, two cases are selected to represent the outage costs in this study. Urban areas are assumed to experience higher outage costs when the power distribution system fails, mainly due to the population density and the high cost of living. Therefore, the outage cost for rural areas is assumed to 50% of the total maintenance expenses (Case A), while the outage cost for urban areas is assumed to 75% of the total maintenance expenses (Case B). The expected outage cost of the distribution pole is calculated based on the following:

$$C_{Out}(t) = \sum_{i=1}^{L} E_i M_T z(t) P_f(t)$$
 and  $M_T = M + C_R$  (41)

where  $E_i$  is a constant equal to 0.5 and 0.75 for the two cases, respectively; and  $M_T$  is the total maintenance expense.

## 6.4. LCC results

Combining the two scenarios described in the failure cost section and the two cases highlighted for the outage cost, a total of four different possible situations are analyzed in this study:

- Case 1A: Full pole decay over time in rural areas
- Case 1B: Full pole decay over time in urban areas
- Case 2A: Pole decay and restoration over time in rural areas
- Case 2B: Pole decay and restoration over time in urban areas

The value of the cost of each component and the total life-cycle cost for Case 2B are shown in Table 3, and the normalized failure costs for all scenarios for different classes with guy has been shown in Fig. 17. Fig. 18 shows the total life cycle cost for different classes of poles without guy and the class 4 with guy. As shown in Fig. 18, installing a

guy cable on the pole yields the lowest LCC among the listed mitigation methods, reducing the life-cycle cost to approximately 25% for class 3 poles.

#### 7. Conclusions

This paper describes a probabilistic performance assessment method for different classes of distribution poles and the impact of the hazard mitigation strategies on enhancing the pole performance. The first step was the characterization of the hazard. The K-S test was performed on the ultimate 3-second gust-design wind speed from ASCE 7 to identify the best distribution, and LHS was used to efficiently generate the sample mean wind speed data. From the generated sample, a wind load model was established using the one-dimensional multivariable stochastic process. The second step in the proposed framework established a finite element model of the distribution systems, composed of three 12.2 m Southern Yellow Pine distribution poles. Using this model combined with the generated wind speeds, a finite element analysis was performed to study the number of wind-induced failures. These events were identified by introducing a bending moment-based failure criterion for the poles. The nominal bending moment was considered as the upper limit of such a failure criterion. However, this value heavily depends on the circumference of the pole itself, which is subject to reduction over time due to aging. In particular, the organic nature of wooden poles makes them prone to decay caused by fungal growth and insect infestation. Based on these considerations, the decay process has a significant effect on the performance of the poles under wind excitation, and its effect was considered in the lifetime vulnerability of the distribution poles. Two main hazard mitigation strategies-guyed distribution poles and the use of a larger class size—were discussed and evaluated. Results showed the significant effect of the mitigation strategies in decreasing the probability of failures and the life-cycle costs of class 3 distribution poles. In particular, the guyed solution proved to be a viable strategy to significantly lowering the total costs during the life of the poles. Although the applicability of such a mitigation solution per this example may not be practical, the methodology presented in this paper could help distribution utilities evaluate design/mitigation options for improved resiliency. Future continuation of this work will center around the validation of the FE analysis through testing, as well as the collection of information on dimensions and configuration variations for the system through surveying.

## Acknowledgments

The research study results reported in this paper was supported by National Science Foundation of USA under Grant No. 1751844. The authors would like to acknowledge and thank the sponsor for their

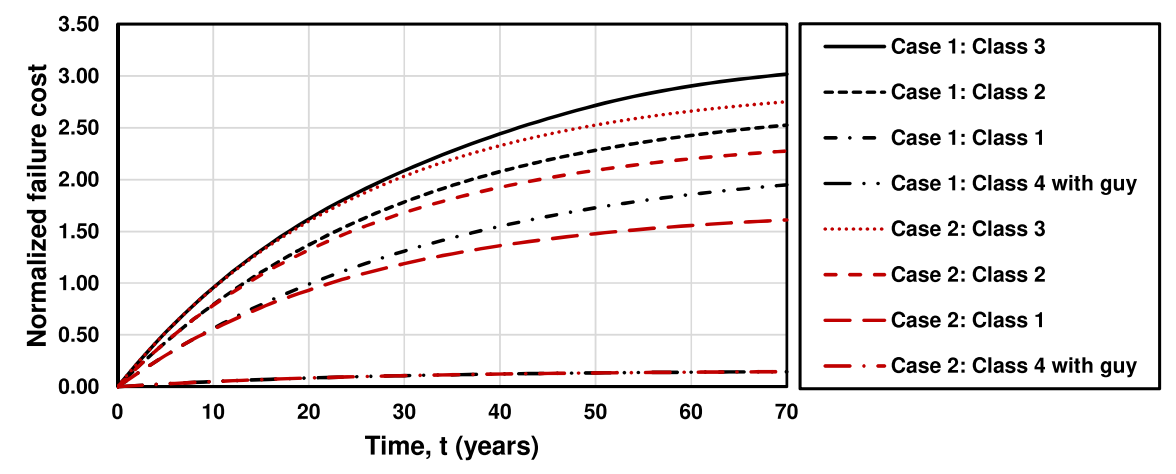


Fig. 17. Normalized failure cost for both scenario for Class 1, 2, 3, and Class 4 with guy.

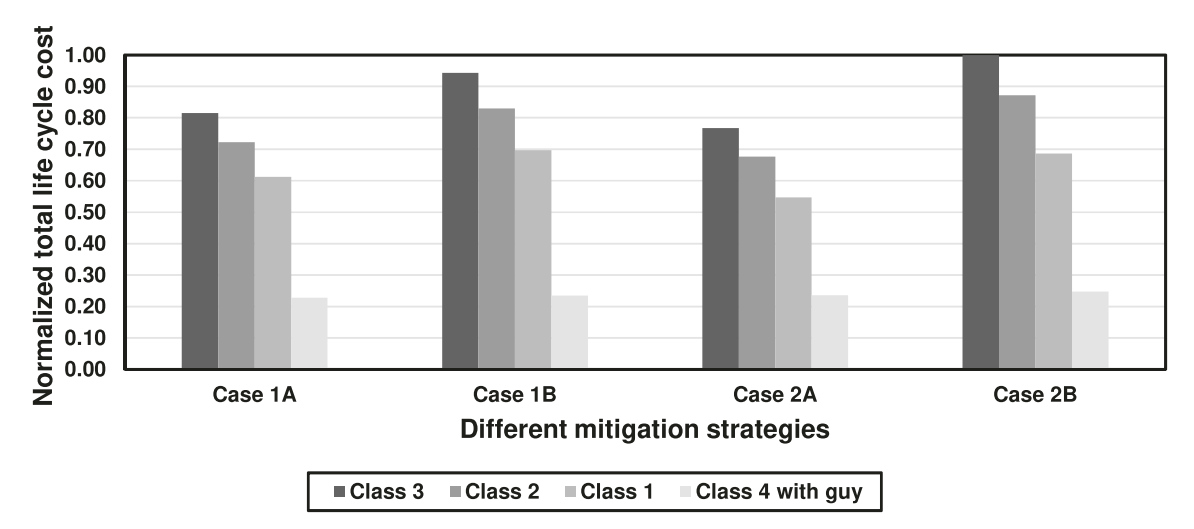


Fig. 18. Normalized total Life Cycle Cost (LLC) Analysis for Class 3, 2, 1 and Guyed Class 4 distribution poles.

support. Opinions and conclusions expressed in this paper are those of the authors and do not necessarily represent those of the National Science Foundation.

#### References

- Campbell RJ. Weather-Related Power Outages and Electric System Resiliency. Congr Res Serv Rep 2012:1–15. R42696.
- [2] Kenward A, Blackout Raja U. Extreme weather, climate change and power outages. Clim Cent 2014;23.
- [3] Weiss, D. and Weidman J. Going to extremes: The \$188 billion price tag from climate-related weather n.d. www.americanprogress.org/issues/ green/news/2013/02/12/52881/going-to-extremes-the-188-billionprice- tag-from-climate-related-extreme-weather/. [accessed January 1, 2017].
- [4] President's council of Economic advisors. Economic Benefits of Increasing Electric Grid Resilience To Weather Outages. Exec Off Pres 2013:1–28.
- [5] Brown R. Cost-Benefit Analysis of the Deployment of Utility Infrastructure Upgrades and Storm Hardening Programs. Raleigh, NC: 2009.
- [6] Graumann A, (U.S.) NCDC, Houston T, Lawrimore J, Levinson D, Lott N, et al. Hurricane Katrina: A Climatological Perspective: Preliminary Report. U.S. Department of Commercee, National Ocanic and Atmospheric Administration, National Environmental Satellite Data and Information Service, National Climatic Data Center; 2005.
- [7] Kwasinski A, Weaver WW, Chapman PL, Krein PT. Telecommunications power plant damage assessment for hurricane katrina{\text{textendash}} site survey and follow-up results. IEEE Syst J 2009;3:277–87. https://doi.org/10.1109/jsyst.2009.2026783.
- [8] Hoffman P, Bryan W, Lippert A. Comparing the Impacts of the 2005 and 2008 Hurricanes on US Energy Infrastructure. United Sates Department of Energy: 2009.
- [9] Liu H, Davidson RA, Rosowsky DV, Stedinger JR. Negative binomial regression of electric power outages in hurricanes. J Infrastruct Syst 2005;11:258–67. https:// doi.org/10.1061/(ASCE)1076-0342(2005) 11:4(258).
- [10] Li J, Dueñas-osorio L, Chen C. Reliability and Controllability of Infrastructure Networks: Do They Match? 12th Int Conf Appl Stat Probab Civ Eng 2015:1–8. http://doi.org/10.14288/1.0076146.
- [11] Ouyang M, Dueñas-Osorio L. Multi-dimensional hurricane resilience assessment of electric power systems. Struct Saf 2014;48:15–24. https://doi.org/10.1016/j. strusafe.2014.01.001.
- [12] Winkler J, Dueñas-Osorio L, Stein R, Subramanian D. Performance assessment of topologically diverse power systems subjected to hurricane events. Reliab Eng Syst Saf 2010;95:323–36. https://doi.org/10.1016/j.ress.2009.11.002.
- [13] Testa AC, Furtado MN, Alipour A. Resilience of coastal transportation networks faced with extreme climatic events. vol. 2532. 2015. http://doi.org/10.3141/ 2532-04.
- [14] Furtado M, Alipour A. Cost assessment of highway bridge network subjected to extreme seismic events. Transp Res Rec J Transp Res Board 2014;2459:29–36. https://doi.org/10.3141/2459-04.
- [15] Bjarnadottir S, Li Y, Stewart MG. Risk-based economic assessment of mitigation strategies for power distribution poles subjected to hurricanes. Struct Infrastruct Eng 2014;10:740–52. https://doi.org/10.1080/15732479.2012.759240.
- [16] Ryan PC, Stewart MG, Spencer N, Li Y. Reliability assessment of power pole infrastructure incorporating deterioration and network maintenance. Reliab Eng Syst Saf 2014;132:261–73. https://doi.org/10.1016/j.ress.2014.07.019.
- [17] Shafieezadeh A, Onyewuchi UP, Begovic MM, Desroches R. Age-dependent fragility models of utility wood poles in power distribution networks against extreme wind hazards. IEEE Trans Power Deliv 2014;29:131–9. https://doi.org/10.1109/tpwrd. 2013.2281265.
- [18] Asian Development Bank. Climate Risk and Adaptation in the Electric Power Sector.

- Mandaluyong City, PHL: Asian Development Bank; n.d.
- [19] Brockett PL, Wang M, Weather Yang C. Derivatives and Weather Risk Management. Risk Manag < html\_ent Glyph = "@amp;". Ascii = "&"/ > Insur Rev 2005;8:127–40. https://doi.org/10.1111/j.1540-6296.2005.00052.x.
- [20] Douglas E, Jacobs J, Hayhoe K, Silka L, Daniel J, Collins M, et al. Progress and challenges in incorporating climate change information into transportation research and design. J Infrastruct Syst 2017. https://doi.org/10.1061/(ASCE)IS.1943-555X. 0000377.
- [21] Entergy. Building a Resilient Energy Gulf Coast: Executive Report 2010:1-11.
- [22] Foedinger R, Boozer JF, Bronstad ME, Davidson JW. Development of energy-absorbing composite utility pole. Transp Res Rec J Transp Res Board 2003;1851:149–57. https://doi.org/10.3141/1851-15.
- [23] Wolfe RW, Moody RC. ANSI Pole Standards: Development and Maintenance. In: Barnes HM, Amburgey TL, editors. Proc. First Southeast. Pole Conf., Madison, WI: Forest Products Society; 1994, p. 143–9.
- [24] Ibrahim S, Polyzois D, Hassan SK. Development of glass fiber reinforced plastic poles for transmission and distribution lines. Can J Civ Eng 2000;27:850–8. https://doi.org/10.1139/199-089.
- [25] Bakis CE, Bank LC, Brown VL, Cosenza E, Davalos JF, Lesko JJ, et al. Fiber-re-inforced polymer composites for construction{\text{textemdash}}state-of-the-art review. J Compos Constr 2002;6:73–87. https://doi.org/10.1061/(asce)1090-0268(2002) 6:2(73).
- [26] Bolin CA, Smith ST. Life cycle assessment of pentachlorophenol-treated wooden utility poles with comparisons to steel and concrete utility poles. Renew Sustain Energy Rev 2011;15:2475–86. https://doi.org/10.1016/j.rser.2011.01.019.
- [27] Datla SV, Pandey MD. Estimation of life expectancy of wood poles in electrical distribution networks. Struct Saf 2006;28:304–19. https://doi.org/10.1016/j. strusafe.2005.08.006.
- [28] Committee AS. 2017 National Electrical Safety Code (NESC). Institute of Electrical and Electronics Engineers ({IEEE}); 2017.
- [29] Vickery PJ, Wadhera D, Galsworthy J, Peterka Ja, Irwin Pa, Griffis La. Ultimate wind load design gust wind speeds in the united states for use in {ASCE}-7. J Struct Eng 2010;136:613–25. https://doi.org/10.1061/(asce)st.1943-541x.0000145.
- [30] Stein M. Large sample properties of simulations using latin hypercube sampling. Technometrics 1987;29:143–51. https://doi.org/10.1080/00401706.1987. 10488205.
- [31] Shinozuka M, Deodatis G, Shinozyka M, Deodatis G. Simulation of stochastic processes by spectral representation. Appl Mech Rev 1991;44:191. https://doi.org/10.1115/1.3119501.
- [32] Shinozuka M, Jan C-M. Digital simulation of random processes and its applications. J Sound Vib 1972;25:111–28. https://doi.org/10.1016/0022-460x(72)90600-1.
- [33] Deodatis G. Simulation of ergodic multivariate stochastic processes. J Eng Mech 1996;122:778–87. https://doi.org/10.1061/(asce)0733-9399(1996) 122:8(778).
- [34] Kaimal JC, Wyngaard JC, Izumi Y, Coté OR. Spectral characteristics of surface-layer turbulence. Q J R Meteorol Soc 1972;98:563–89. https://doi.org/10.1002/qj. 49709841707.
- [35] Davenport AG. The dependence of wind loads on meteorological parameters. Proc Int Res Semin Wind Eff Build Struct. University of Toronto Press; 1967. p. 19–82.
- [36] Simiu E, Scanlan RH. Wind effects on structures: an introduction to wind engineering. New York: Wiley; 1986.
- [37] Hayes MH. Statistical digital signal processing and modeling. New York: John Wiley & Sons; 1996.
- [38] Accredited Standards Committee. Wood poles specifications and dimensions. Washington, DC: 2015.
- [39] American National Standard. Solid Sawn-Wood Crossarms and Braces -Specification and Dimensions (ANSI O5.3). Washington, DC: Alliance for Telecomunications Industry Solutions; 2002.
- [40] Yang SC, Hong HP. Nonlinear inelastic responses of transmission tower-line system under downburst wind. Eng Struct 2016;123:490–500. https://doi.org/10.1016/j.

- engstruct.2016.05.047.
- [41] Short TA. Electric power distribution equipment and systems. Boca Raton, FL: Taylor & Francis: 2006.
- [42] Elliot JF. Unguyed Distribution Poles Strength Requirements. 2014.
- [43] Gezer ED, Temiz A, Yüksek T. Inspection of wooden poles in electrical power distribution networks in Artvin, Turkey. Adv Mater Sci Eng 2015;2015:1–11. https://doi.org/10.1155/2015/659818.
- [44] Lee Willis H, Romero-aguero J, Hammett W. Distribution wood pole managment practices in the electric. Utility. 2012.
- [45] Baraneedaran S, Gad EF, Flatley I, Kamiran A, Wilson JL, others. Review of inservice assessment of timber poles. Proc Aust Earthq Eng Soc Newcastle 2009.
- [46] Bjarnadottir S, Li Y, Stewart MG. Hurricane risk assessment of power distribution poles considering impacts of a changing climate. J Infrastruct Syst 2013;19:12–24. https://doi.org/10.1061/(asce)is.1943-555x.0000108.
- [47] Wang C-H, Leicester RH, Nguyen M. Probabilistic procedure for design of untreated timber poles in-ground under attack of decay fungi. Reliab Eng Syst Saf 2008;93:476–81. https://doi.org/10.1016/j.ress.2006.12.007.
- [48] Elgohary N. Wood Pole Inspection and Maintenance. 2013.
- [49] Li Y, Yeddanapudi S, McCalley JD, Chowdhury AA, Moorehead M. Degradation-path model for wood pole asset management. In: Proc 37th Annu North Am Power Symp 2005. IEEE; n.d. http://doi.org/10.1109/naps.2005.1560538.
- [50] Wang C, Leicester RH, Nguyen MN. Decay in Ground Contact. Highett, Victoria: 2008.
- [51] Shinozuka M, Feng MQ, Lee J, Naganuma T, Of N, By U, et al. Statistical analysis of fragility curves. J Eng Mech 2000;126:1224–31. https://doi.org/10.1061/(asce) 0733-9399(2000) 126:12(1224).
- [52] Brown RE. Hurricane hardening efforts in Florida. 2008 (IEEE) Power Energy Soc Gen Meet - Convers Deliv Electr Energy 21st Century, IEEE; 2008. http://doi.org/

- 10.1109/pes.2008.4596940.
- [53] Miller MD, Wong JC. Guidelines for electrical transmission line structural loading. 2009. http://doi.org/10.1061/9780784410356.
- [54] Supply USS. USS Tiger Brand Wire Rope Engineering Handbook. U.S. Steel Supply; 1976.
- [55] Union. Product catalog: galvanized strand n.d.
- [56] American Society of Civil Engineers (ASCE). Design of Guyed Electrical Transmission Structures. American Society of Civil Engineers; 1997. http://doi.org/ 10.1061/9780784402849.
- [57] Alipour A, Shafei B, Shinozuka M. Performance evaluation of deteriorating highway bridges located in high seismic areas. J Bridg Eng 2011;16. https://doi.org/10. 1061/(ASCE)BE.1943-5592.0000197.
- [58] Alipour A, Shafei B, Shinozuka MS. Capacity loss evaluation of reinforced concrete bridges located in extreme chloride-laden environments. Struct Infrastruct Eng 2013;9:8–27. https://doi.org/10.1080/15732479.2010.525243.
- [59] Rose A, Porter K, Dash N, Bouabid J, Huyck C, Whitehead J, et al. Benefit-Cost Analysis of FEMA Hazard Mitigation Grants. Nat Hazards Rev 2007;8:97–111. https://doi.org/10.1061/(asce)1527-6988(2007) 8:4(97).
- [60] Mankowski M, Hansen E, Morrell J. Wood pole purchasing, inspection, and maintenance: A survey of utility practices. For Prod J 2002;52:43.
- [61] Osmose Utilities Services. Best Practices in Wood Pole Plant Management. 2014.
- [62] Cui W, Caracoglia L. Simulation and analysis of intervention costs due to wind-induced damage on tall buildings. Eng Struct 2015;87:183–97. https://doi.org/10.1016/j.engstruct.2015.01.001.
- [63] Ierimonti L, Caracoglia L, Venanzi I, Materazzi AL. Investigation on life-cycle damage cost of wind-excited tall buildings considering directionality effects. J Wind Eng Ind Aerodyn 2017;171:207–18. https://doi.org/10.1016/j.jweia.2017.09.020.
- [64] Personal communication with Iowa Department of Homeland Security. n.d.